energies

MDPI

Article

Multi-Objective Optimization Design for Indirect Forced-Circulation Solar Water Heating System Using NSGA-II

Myeong Jin Ko

Received: 8 September 2015 ; Accepted: 10 November 2015 ; Published: 19 November 2015
Academic Editor: Timothy Anderson

Urban Development Institute, Incheon National University, Incheon 406-772, Korea; whistlemj@nate.com; Tel.: +82-32-835-4656

Abstract: In this study, the multi-objective optimization of an indirect forced-circulation solar water heating (SWH) system was performed to obtain the optimal configuration that minimized the life cycle cost (LCC) and maximized the life cycle net energy saving (LCES). An elitist non-dominated sorting genetic algorithm (NSGA-II) was employed to obtain the Pareto optimal solutions of the multi-objective optimization. To incorporate the characteristics of practical SWH systems, operation-related decision variables as well as capacity-related decision variables were included. The proposed method was used to conduct a case study wherein the optimal configuration of the SWH system of an office building was determined. The case study results showed that the energy cost decreases linearly and the equipment cost increases more significantly as the LCES increases. However, the results also showed that it is difficult to identify the best solution among the Pareto optimal solutions using only the correlation between the corresponding objective function values. Furthermore, regression analysis showed that the energy and economic performances of the Pareto optimal solutions are significantly influenced by the ratio of the storage tank volume to the collector area (RVA). Therefore, it is necessary to simultaneously consider the trade-off and the effect of the RVA on the Pareto optimal solutions while selecting the best solution from among the optimal solutions.

Keywords: solar water heating system; multi-objective optimization; life cycle cost; life cycle net energy saving; non-dominated sorting genetic algorithm; Pareto optimal solution

1. Introduction

Over the past several decades, a number of design methods have been developed for solar water heating (SWH) systems, ranging from correlation-based methods such as the ϕ method [1], $\overline{\phi}$ method [2], f-chart method [3], and $\overline{\phi}$, f-chart method [4] to simulation-based methods such as transient system simulation (TRNSYS) [5] and pre-design and optimization tool for solar heating systems with seasonal storage (SOLCHIP) [6]. In recent years, some design methods using optimization techniques such as linear and nonlinear optimization and evolutionary algorithms have been proposed. These optimization-based methods are conceptually different from traditional correlation- and simulation-based methods in terms of the process of finding the optimal design. Most of them are based on certain characteristics and behavior of biological and molecular systems, swarms of insects, or neurobiological systems [7]. For instance, to optimize the design variables of an SWH system, linear and nonlinear optimization methods [8,9], genetic algorithms (GAs) [7,10–15], and particle swarm optimization (PSO) [16,17] have been applied. Furthermore, hybrid optimization techniques such as the combination of PSO with the Hooke-Jeeves method [18] and the combination of a GA with the binary search method [19] have also been utilized in recent years.

A majority of these studies have determined the optimal size of SWH systems by choosing various design criteria as the objective functions, including the annual system efficiency [8], annual solar fraction [20,21], life cycle savings [12,22], life cycle cost (LCC) [14,15,23,24], annualized LCC [25,26], and payback period [9,10,13]. For instance, Krause *et al.* [11] proposed a method to minimize the solar heat cost of an existing large solar thermal system. Loomans *et al.* [10] applied a GA to minimize the payback time of large solar hot water systems. Kalogirou [12] employed a GA to estimate the optimum collector area and tank volume for maximizing life cycle savings. Kim *et al.* [13] also optimized SWH systems through the minimization of the capital payback period. Hobbi *et al.* [21] studied the optimal design of a forced-circulation SWH system by maximizing the annual efficiency and solar fraction. Kulkarni *et al.* [25] proposed the "design space methodology" to design an SWH system by minimizing the annualized LCC. Ko [15] employed a GA to optimize the capacity and operation-related design variables of an indirect forced-circulation SWH system for minimizing the LCC.

In previous studies, SWH systems have been designed by optimizing one particular objective function. Consequently, the optimal design of a system will differ depending on the objective functions that the researchers and engineers consider as the key design criteria. In addition, most real-world search and optimization problems naturally involve multiple objectives [27], and so do the design problems of SWH systems. Therefore, single-objective optimization frequently leads to unacceptable solutions with respect to the other objectives when the objectives under consideration produce trade-offs with each other and the rest of the objectives are also important. For many complicated problems, multi-objective approaches are more accurate and real because they allow decision makers to think about the trade-offs between different benefits of different objectives [28]. In recent years, therefore, multi-objective optimization has been widely used to design solar thermal-driven systems such as solar-driven heat engine systems [29,30], solar-driven heat pumps [31], solar-driven absorption cooling systems [32,33], and solar-driven hybrid cooling, heating, and power systems [34–36]. However, only a few studies have considered the multi-objective optimization of a forced-circulation SWH system.

Therefore, in this study, the multi-objective optimization of an indirect forced-circulation SWH system is carried out to determine the optimal configuration based on energy and economic aspects. The collector size, storage tank, heat exchanger, auxiliary heater, collector slope, and mass flow rates on the hot and cold sides of a heat exchanger are selected as the decision variables. An elitist non-dominated sorting genetic algorithm (NSGA-II) is used to obtain the Pareto optimal solutions by minimizing the LCC and maximizing the life cycle net energy saving (LCES) of an SWH system. As a case study, the proposed multi-objective optimization method is applied to determine the optimal configuration of the SWH system of an office building. This study evaluates the trade-off between the non-dominated solutions obtained from the case study through the regression technique. The effect of the ratio of the storage tank volume to the collector area (RVA) on the energy and economic performance of the non-dominated solutions is also assessed.

2. Mathematical Models of SWH System

Figure 1 shows the schematic diagram of an indirect forced-circulation SWH system. The SWH system mainly consists of flat-plate solar collectors, an external heat exchanger, a storage tank, auxiliary heaters, circulation pumps, and a differential temperature controller (DTC). This SWH system has two circulation circuits: a primary circuit that collects the solar energy and transfers it to the storage tank via the external heat exchanger and a secondary circuit that transfers the heat stored in the storage tank to the load. The two circulation pumps in the primary circuit are controlled using the DTC. The auxiliary heaters are added to match the energy requirement of the hot water load when the storage tank temperature does not reach the desired temperature.

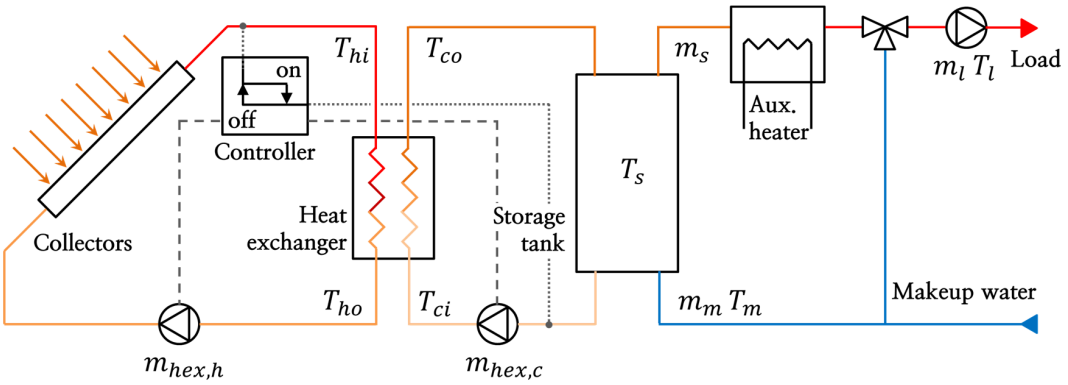

Figure 1. Schematic diagram of indirect forced-circulation SWH system used in this study.

2.1. Flat-Plate Solar Collector

Solar collectors absorb solar radiation and convert it into thermal energy. According to the isotropic diffuse model, the solar radiation on a tilted collector surface can be evaluated from the following equation [37]:

$$I_T = I_b R_b + I_d \left[\frac{1+cos\,(\beta_{coll})}{2}\right] + I\rho_g \left[\frac{1-cos\,(\beta_{coll})}{2}\right] \tag{1}$$

where I_T is the hourly total solar radiation on the tilted collector array (W/m^2); I_b, I_d, and I are the hourly beam, diffuse, and global radiation on a horizontal surface, respectively (W/m^2); R_b is the ratio of the beam radiation on the tilted surface to that on a horizontal surface; ρ_g is the ground reflectance; and β_{coll} is the slope of the collector array (°).

Over the operation period, the useful heat gain of identical solar collectors connected in series is given by the following equation:

$$q_u = \gamma_o A_{coll} N_{coll,s} \left[F_R\,(\tau\alpha)\, I_T - F_R U_L\,(T_{ho} - T_a)\right] \tag{2}$$

where A_{coll} is the gross area of a single collector module (m^2); $N_{coll,s}$ is the number of identical collectors connected in series; $F_R\,(\tau\alpha)$ and $F_R U_L$ are the intercept and slope of the efficiency curve of identical collector modules connected in series, respectively; T_{ho} is the hot stream outlet temperature of the heat exchanger (°C); T_a is the outdoor dry-bulb temperature (°C); and γ_o is the output control function of the DTC.

For identical collector modules connected in series, the intercept and slope of the efficiency curve can be estimated by the following equations [37]:

$$F_R\,(\tau\alpha) = F_{R1}\,(\tau\alpha)_1 \left[\frac{1-\left(1-\frac{A_{coll}F_{R1}(\tau\alpha)_1}{A_{coll}m_{coll,u}c_{p,c}}\right)^{N_{coll,s}}}{N_{coll,s}\frac{A_{coll}F_{R1}(\tau\alpha)_1}{A_{coll}m_{coll,u}c_{p,c}}}\right] \tag{3}$$

$$F_R U_L = F_{R1} U_{L1} \left[\frac{1-\left(1-\frac{A_{coll}F_{R1}(\tau\alpha)_1}{A_{coll}m_{coll,u}c_{p,c}}\right)^{N_{coll,s}}}{N_{coll,s}\frac{A_{coll}F_{R1}(\tau\alpha)_1}{A_{coll}m_{coll,u}c_{p,c}}}\right] \tag{4}$$

where $F_{R1}\,(\tau\alpha)_1$ and $F_{R1}U_{L1}$ are the intercept and slope of the efficiency curve of a single collector, respectively; $m_{coll,u}$ is the mass flow rate per unit area of the collector fluid (kg/s· m^2); and $C_{p,c}$ is the specific heat of the collector fluid (J/kg· °C).

2.2. Heat Exchanger

The external heat exchanger is used to keep the fluid of the SWH system separate while allowing solar heat to transfer from the collector fluid (*i.e.*, antifreeze fluid) in the primary circuit to the water in the secondary circuit. In the proposed method, the counter-flow-type heat exchanger is used and its number is fixed as one. The effectiveness-number of exchanger heat transfer units(NTU) method is used to calculate the solar energy transferred from the collector array to the storage tank via the external heat exchanger. This method uses three dimensionless parameters: heat exchanger effectiveness (ε), NTU, and capacity rate ratio (c_r). For a given counter-flow-type heat exchanger, these three parameters are generally expressed as follows [37]:

$$\varepsilon = \begin{cases} \frac{1-exp[-NTU(1-c_r)]}{1-c_r exp[-NTU(1-c_r)]}, & c_r \neq 1 \\ \frac{NTU}{NTU+1}, & c_r = 1 \end{cases} \tag{5}$$

$$c_r = \frac{C_{hex,min}}{C_{hex,max}} \tag{6}$$

$$NTU = \frac{UA_{hex}}{C_{hex,min}} \tag{7}$$

$$C_{hex,c} = m_{hex,c} C_{p,w} \tag{8}$$

$$C_{hex,h} = A_{coll} m_{coll,u} N_{coll,p} C_{p,c} \tag{9}$$

$$C_{hex,min} = min\left(C_{hex,c}, C_{hex,h}\right) \tag{10}$$

$$C_{hex,min} = max\left(C_{hex,c}, C_{hex,h}\right) \tag{11}$$

where $m_{hex,c}$ is the mass flow rate on the cold side of the heat exchanger (kg/s); $C_{p,w}$ is the specific heat of water (J/kg·°C); $N_{coll,p}$ is the number of parallel connections in the collector array; $C_{hex,c}$ and $C_{hex,h}$ are the capacity rates of fluids on the hot and cold sides of the heat exchanger, respectively; and UA_{hex} is the overall heat transfer coefficient-area product of the heat exchanger (W/°C).

Therefore, the heat transfer rate and the outlet temperatures on the hot and cold sides of the heat exchanger can be determined as follows:

$$q_{hex} = \begin{cases} \varepsilon C_{hex,h} \left(T_{hi} - T_{ci}\right) \gamma_o, & C_{hex,min} = C_{hex,h} \\ \varepsilon C_{hex,c} \left(T_{hi} - T_{ci}\right) \gamma_o, & C_{hex,min} = C_{hex,c} \end{cases} \tag{12}$$

$$T_{ho} = T_{hi} - \frac{q_{hex}}{C_{hex,h}} \tag{13}$$

$$T_{co} = T_{ci} + \frac{q_{hex}}{C_{hex,c}} \tag{14}$$

where T_{hi} is the hot stream inlet temperature of the heat exchanger (°C) and T_{ci} and T_{co} are the cold stream inlet and outlet temperatures of the heat exchanger (°C).

2.3. Storage Tank

The proposed method uses a mathematical model considering the mass and energy balance of a well-mixed storage tank. At any instant of time, the energy balance of a well-mixed storage tank can be described as follows [25]:

$$\left(\rho_w C_{p,w} V_s\right) \frac{dT_s}{dt} = q_{hex} - q_{Ls} - q_l - q_d \tag{15}$$

where ρ_w is the density of water (kg/m^3); V_s is the volume of the storage tank (m^3); and q_l, q_d, and q_{Ls} are the heat loss of the storage tank (W), heat discharged to avoid overheating of the storage tank (W), and solar energy extracted from the storage tank (W), respectively.

The solar energy supplied from the storage tank to the load (q_{Ls}) can be estimated as follows:

$$q_{Ls} = m_s C_{p,w} \left(T_s - T_m\right) \gamma_o \tag{16}$$

with

$$m_s = \begin{cases} m_l \left(\frac{T_l - T_m}{T_s - T_m}\right), \ T_s > T_l \\ m_l, \ T_s \leqslant T_l \end{cases} \tag{17}$$

where m_s is the mass flow rate from the storage tank to the load (kg/s); m_l, the mass flow rate of the desired hot water load (kg/s); T_l, the desired hot water temperature; and T_m, the makeup water temperature (°C).

Meanwhile, the energy loss from the storage tank (q_l) to the surroundings can be expressed as follows:

$$q_l = U_s A_s \left(T_s - T_{amb}\right) \tag{18}$$

where U_s and A_s are the heat loss coefficient (W/m$^2\cdot$°C) and surface area (m^2) of the storage tank, respectively, and T_{amb} is the ambient temperature (°C).

The method proposed in this paper is developed to design an SWH system for low-temperature applications. Therefore, if the storage tank temperature is greater than the maximum allowable temperature, the surplus heat will be discharged to avoid overheating. The discharged heat and flow rate can be estimated as follows:

$$q_d = \begin{cases} m_d C_{p,w} \left(T_s - T_{s,max}\right), \ T_s > T_{s,max} \\ 0, \ T_s \leqslant T_{s,max} \end{cases} \tag{19}$$

$$m_d = \begin{cases} \frac{\rho_w V_s \left(T_s - T_{s,max}\right)}{\left(T_s - T_m\right)}, \ T_s > T_{s,max} \\ 0, \ T_s \leqslant T_{s,max} \end{cases} \tag{20}$$

where m_d is the mass flow rate of the discharged water from the storage tank (kg/s) and $T_{s,max}$ is the maximum allowable temperature of the storage tank (°C).

The parameters of the indirect forced-circulation SWH system given by Equations (1)–(20) are evaluated based on the initial temperature of the storage tank at any time step. To continuously calculate these parameters on an hourly basis, the final temperature of the storage tank at the end of any time step must be known because it will be the initial temperature for the next time step. The final temperature of the storage tank can be determined as follows:

$$T_{s,f} = T_s + \frac{\left(q_{hex} - q_{Ls} - q_l - q_d\right) 3,600}{\rho_w C_{p,w} V_s} \Delta t \tag{21}$$

where $T_{s,f}$ is the final temperature of the storage tank at the end of any time step (°C).

2.4. Auxiliary Heater

The obtained solar energy does not always match the energy required by the hot water because solar radiation varies according to the weather and time of day. Therefore, auxiliary heaters are needed as back-up heat sources. The auxiliary heating energy can be estimated as follows:

$$q_{aux} = \begin{cases} 0, \ T_s > T_l \\ m_l C_{p,w} \left(T_l - T_s\right), \ T_s \leqslant T_l \end{cases} \tag{22}$$

The energy consumption of the auxiliary heaters is calculated using a simple model, and their overall efficiency, part load ratio, and energy input ratio are shown below [38]:

$$PLR_{aux} = \frac{q_{aux}}{q_{aux,total}} \tag{23}$$

$$EIR\left(PLR_{aux}\right) = a + bPLR_{aux} + cPLR_{aux}{}^2 + dPLR_{aux}{}^3 \tag{24}$$

$$F_{LNG} = \frac{q_{aux}EIR\left(PLR_{aux}\right)}{PLR_{aux}\eta_{aux}Q_{LNG,LHV}} \tag{25}$$

where PLR_{aux} is the part load ratio of the auxiliary heaters at each time step; $q_{aux,total}$ is the heating capacity of the auxiliary heaters (W); $EIR\left(PLR_{aux}\right)$ is the energy input ratio of the auxiliary heaters; a, b, c, and d are the coefficients for the energy input ratio (a = 0.0080472574, b = 0.87564457, c = 0.29249943, and d = −0.17624156); F_{LNG} is the hourly liquid natural gas (LNG) consumption (m^3); η_{aux} is the overall efficiency of the auxiliary heater; and $Q_{LNG,LHV}$ is the lower heating value of LNG (W/m^3).

2.5. Circulation Pump

The indirect forced-circulation SWH system considered in this study requires two pumps that are turned on or off by the DTC. The electricity consumption of the circulation pumps is calculated using the simple model shown below:

$$F_{ELE} = \gamma_o \frac{m_{fluid}gH_p}{\eta_p\eta_m} \tag{26}$$

where F_{ELE} is the electricity consumption of the circulation pump (W); m_{fluid}, the flow rate of the fluid passing through the pump (kg/s); g, the acceleration due to gravity (m/s^2); H_p, the pump head (m); η_p, the pump efficiency; and η_m, the motor efficiency.

2.6. Energy Performance of SWH System

When evaluating the energy performance of an SWH system over a given time horizon, the most widely used performance indicators include the solar fraction and efficiency of the solar system, which are respectively described by Equations (27) and (28):

$$F_S = 1 - \sum_1^t \frac{q_{aux}\left(t\right)}{q_L\left(t\right)} \tag{27}$$

$$\eta_{sys} = \sum_1^t \left[q_{Ls}\left(t\right) - PEF_{ELE} \times F_{ELE}\left(t\right)\right] / \sum_1^t \left[A_{coll} \times N_{coll} \times I_T\left(t\right)\right] \tag{28}$$

where q_L is the hourly hot water load; PEF_{ELE} is the primary energy factor for electricity; N_{coll} is the number of solar collectors; and F_S and η_{sys} are the solar fraction and efficiency of the solar system over a given time horizon, respectively.

3. Multi-Objective Optimization Method of SWH System

3.1. Decision Variable

The proposed multi-objective optimization method is developed to determine the optimal design of an indirect forced-circulation SWH system based on the minimization of the LCC and maximization of the LCES. To obtain an efficient and reasonable design, installation- and operation-related design variables as well as capacity-related design variables are optimized. The sizes of the main components except for the heat exchanger and storage tank, whose quantity is fixed

as one, are computed using their quantity and unit capacity. The unit capacities of each component are recognized according to the device types, which are expressed as the identification number assigned in regular sequence in the inputted data tables. Therefore, each design of the SWH system, which acts as a chromosome in a GA process, is described by a decision vector consisting of nine decision variables, as shown below:

$$x = \left(T_{coll}, N_{coll}, T_{hex}, T_{tank}, T_{aux}, N_{aux}, \beta_{coll}, m_{coll,u}, m_{hex,c}\right)^T \tag{29}$$

where T_{coll} is the type of solar collector; T_{hex}, the type of heat exchanger; T_{tank}, the type of storage tank; T_{aux}, the type of auxiliary heater; and N_{aux}, the number of auxiliary heaters.

3.2. Objective Functions

The proposed optimization method is developed to obtain the non-dominated solution of an indirect forced-circulation SWH system by simultaneously maximizing a technical objective and minimizing an economic objective. Many previous studies suggest that SWH systems have the advantages of reduced fossil fuel consumption and environmental pollution throughout their lifetime. Therefore, to quantify these advantages, this study considers the maximization of the LCES as the technical objective function, which is defined as follows:

$$Q_{LCES} = \sum_{t=1}^{8760} \left[q_{Ls}(t) - PEF_{ELE} \times F_{ELE}(t)\right] \times n_p \tag{30}$$

where Q_{LCES} is the LCES of the SWH system over the planning period and n_p is the planning period.

The economic objective function is evaluated by minimizing the LCC, which includes all the costs—the initial cost (C_I), maintenance cost (C_M), replacement cost (C_R), energy cost (C_E), and subsidy cost (C_S)—incurred during the entire planning period [15]. This objective function can be described by Equation (31). In addition, C_I, C_M, C_R, C_E, and C_S are calculated by Equations (32)–(35), and (37), respectively.

$$C_{LCC} = C_I + C_M + C_R + C_E - C_S \tag{31}$$

$$C_I = \left(C_{coll,j}N_{coll} + C_{hex,j} + C_{tank,j} + C_{aux,j}N_{aux}\right)(1 + R_I) \tag{32}$$

$$C_M = C_I R_M \left[\frac{(1+i)^{n_p} - 1}{i(1+i)^{n_p}}\right] \tag{33}$$

$$C_{R,c} = \sum_{n_{r,c}=1}^{n_{r,c}} \left\{C_{I,c}\left[\frac{1}{(1+i)^{(n_{l,c}n_{r,c})}}\right]\right\} \tag{34}$$

$$C_E = \sum_{t=1}^{8,760} \left[c_{ELE}(t) F_{ELE}(t)\right] UPA^*_{ELE} + \sum_{t=1}^{8,760} \left[c_{LNG}(t) F_{LNG}(t)\right] UPA^*_{LNG} \tag{35}$$

$$UPA^*_{fuel} = \frac{\left(\frac{1+e_{fuel}}{1+i}\right)\left[\left(\frac{1+e_{fuel}}{1+i}\right)^{n_p} - 1\right]}{\left(\frac{1+e_{fuel}}{1+i}\right) - 1} \tag{36}$$

$$C_s = \begin{cases} C_I R_S, & A_{R,max} > A_{coll,j}N_{coll,j} \\ \left[C_{coll,j}\,floor\left(\frac{A_{R,max}}{A_{coll,j}}\right) + C_{hex,j} + C_{tank,j} + C_{aux,j}N_{aux,j}\right](1 + R_I)R_S, & A_{R,max} \leqslant A_{coll,j}N_{coll,j} \end{cases} \tag{37}$$

where $C_{coll,j}$, $C_{hex,j}$, $C_{tank,j}$, and $C_{aux,j}$ are the purchase prices of the jth solar collector, heat exchanger, storage tank, and auxiliary heater, respectively; R_I is the percentage of the supplementary cost against the direct purchase cost; R_M is the percentage of the annual maintenance cost against the initial cost; $C_{R,c}$ and $C_{I,c}$ are the replacement and initial costs of each component, respectively; n_p is the planning

period; $n_{l,c}$ is the lifetime of each component; $n_{r,c}$ is the number of times each component is replaced; i is the real discount rate; UPA^*_{ELE} and UPA^*_{LNG} are the uniform present value factors adjusted to reflect the electricity and LNG price escalation rates, respectively; c_{ELE} and c_{LNG} are the hourly electricity cost (KRW/kW·h) and hourly LNG cost (KRW/m^3) for the SWH system, respectively; F_{ELE} and F_{LNG} are the hourly electricity consumption (kW·h) and hourly LNG consumption (m^3), respectively; e_{fuel} is the fuel price escalation rate; $A_{coll,j}$ is the gross area of the jth solar collector; $A_{R,max}$ is the maximum capacity available to receive the subsidy cost (m^2); and R_S is the percentage of the subsidy cost against the initial cost (%).

3.3. Constraint Conditions

In the proposed optimization method, the constraints can be classified as follows:

(a) The limits of T_{coll}, T_{hex}, T_{tank}, and T_{aux} are set automatically as the number of types in the inputted data tables of each component.

(b) The limits of N_{coll} and N_{aux} are not set because to be a feasible solution, any decision vector should be subject to the inequality constraints (c) and (d) mentioned below. The number of storage tanks and heat exchangers is taken as one because this is the common configuration of indirect forced-circulation SWH systems in South Korea.

(c) To make the solutions obtained by the optimization method reasonable for practical designs, space should be available to install solar collectors. This is defined as follows:

$$N_{coll} W_{coll,j} H_{coll,j} \left[cos\left(\beta\right) + \frac{sin\left(\beta_{coll}\right)}{tan\left(\alpha_{s,w}\right)} \right] \leqslant A_{coll,max} \tag{38}$$

(d) If solar energy is not available, the auxiliary heaters should be capable of providing the required hot water load, as shown below:

$$q_{L,peak} \leqslant q_{aux,j} N_{aux} \tag{39}$$

(e) The slope of the collector array is given as follows:

$$0 \leqslant \beta_{coll} \leqslant 90 \tag{40}$$

(f) Considering the recommended range in previous studies [13,21], the mass flow rates on the hot and cold sides of the heat exchanger should be subject to the following inequality constraints:

$$0.005 \leqslant m_{coll,u} \leqslant 0.025 \tag{41}$$

$$0.5 A_{coll,j} m_{coll,u} N_{coll,p} \leqslant m_{hex,c} \leqslant 2.0 A_{coll,j} m_{coll,u} N_{coll,p} \tag{42}$$

(g) Increasing the NTU value of a heat exchanger beyond three or four usually results in only an insignificant improvement in effectiveness compared to the increase in the cost. Therefore, the NTU of the heat exchanger should be subject to the following constraint:

$$NTU \leqslant 3 \tag{43}$$

where $W_{coll,j}$ and $H_{coll,j}$ are the width and height of the jth solar collector, respectively (m); $\alpha_{s,w}$ is the meridian altitude in winter (°); $A_{coll,max}$ is the space available to install solar collectors (m^2); $q_{L,peak}$ is the peak hot water load (W); and $q_{aux,j}$ is the heating capacity of the jth auxiliary heater (W).

3.4. Application of NSGA-II to Optimize SWH System

A GA is a popular metaheuristic technique that is particularly well suited for the optimal design problems of energy systems [28] and has been proved to be a good method to solve combinatorial

optimization problems in many previous studies [7,10–13]. To optimize the design variables of the SWH system, this study uses the evolutionary algorithm based on NSGA-II proposed by Deb [39,40]. The proposed optimization algorithm is implemented using a hierarchical structure, as shown in Figure 2. The top-down instructions are described as follows:

Step 1: Read input data

In the initial step, the input data for the proposed method consists of the hourly solar radiation, outdoor dry-bulb temperature, and makeup water temperature data; the hourly hot water demands and the technical and economic data of the main components (see the Appendix at the end of this paper); and the design parameters to calculate the objective functions and constraint conditions.

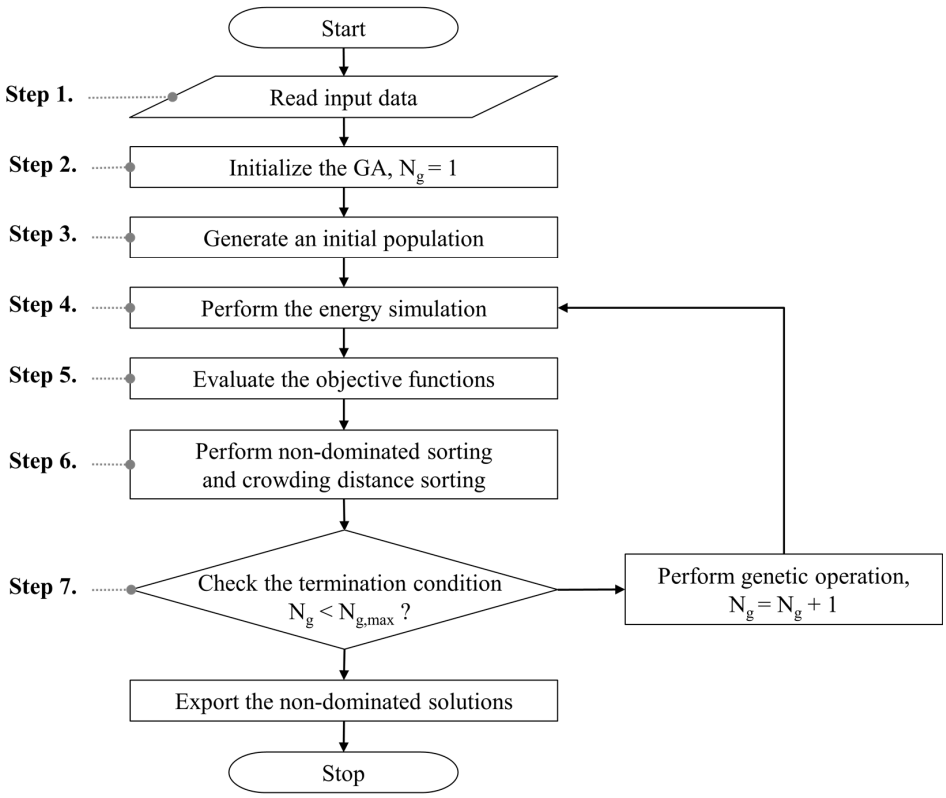

Figure 2. Flowchart of proposed multi-objective optimization algorithm.

Step 2: Initialize the GA

GA parameters such as the population size, number of generations ($N_{g,set}$), crossover probability, and mutation probability are specified. The GA parameters used in this study are as follows: number of generations = 3000, population size = 50, simulated binary crossover probability = 0.9, and polynomial mutation probability = 0.3.

Step 3: Generate an initial population

Then, an initial population, which is a set of possible individuals corresponding to the decision vectors, is randomly generated. If the generated individuals violate any constraints as described in Section 3.3, the individuals are removed, and the possible individuals are randomly regenerated to form an initial population according to the number of the possible individuals as described in Step 2.

Step 4: Perform the energy simulation

All individuals in the population are decoded into their corresponding design of the SWH system and are simulated on an hourly basis using mathematical models as described in Section 2 and the input data loaded in Step 1.

Step 5: Evaluate the objective functions

The objective functions—the LCC and LCES of each individual—are computed based on the mathematical model described in Section 3.2 using the simulation results calculated in Step 4 and data inputted in Step 1.

Step 6: Perform non-dominated sorting and crowding distance sorting

Then, to sort the population according to the level of non-domination based on the values of the objective function, each individual is compared with every other individual in the population. The most widely spread individuals are included in the offspring population to the number of population size by using the crowding distance values, starting with individuals of the first non-dominated front.

Step 7: Check the termination condition

If the iteration number reaches the maximum number of generations set in Step 2, the optimization process is terminated and the non-dominated solutions at the last generation are obtained as the Pareto optimal set. Otherwise, the individuals go through genetic operations such as crossover and mutation, and the algorithm is repeated from Step 3 until the termination condition is satisfied.

4. Simulation Results and Discussion

4.1. Simulation Parameters

The proposed multi-objective optimization method was applied to the design of the indirect forced-circulation SWH system of an office building located in Incheon, South Korea, at Latitude 36°70′ N and Longitude 125°33′. The distribution of daily hot water demand on three different days—a weekday, Saturday, and Sunday—according to the load profile of a typical office building [41] is shown in Figure 3a. Figure 3b shows the hourly hot water load profile over one year, which is used as the input data described in Section 3.4. Figure 4 shows the hourly global horizontal solar irradiance, outdoor air temperature, and makeup water temperature for Incheon. The technical and economic characteristics of the main components used in the case study are summarized in A1–A4 at the end of this paper. Other commercially available devices can be included in the set of devices by designers or researchers. Table 1 lists the design parameters and assumptions considered in the optimization process. Table 2 lists the electricity and LNG tariffs for an office building in South Korea.

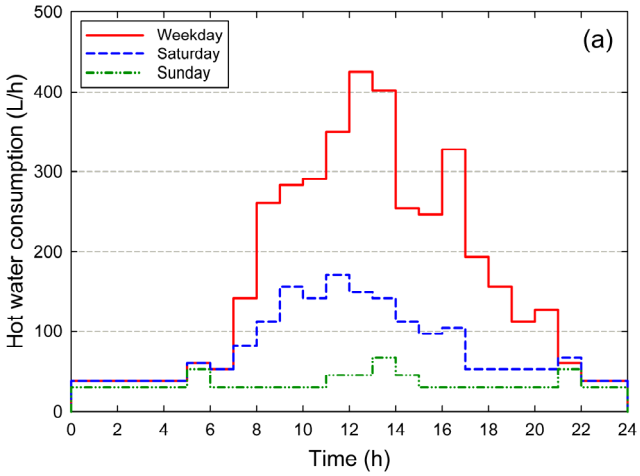

Figure 3. *Cont.*

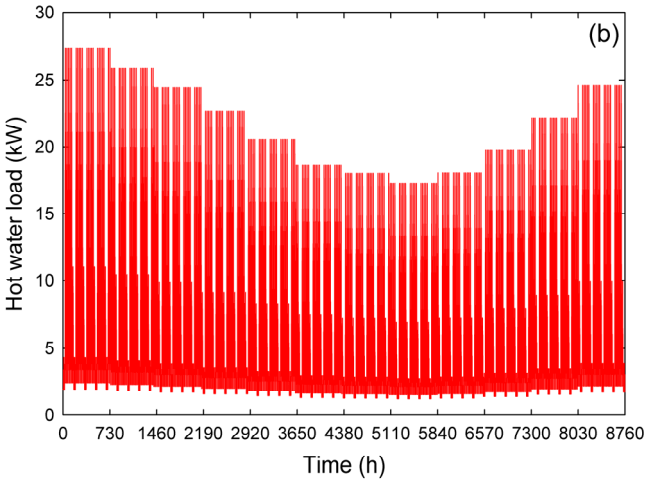

Figure 3. (**a**) Hourly hot water consumption over one day and (**b**) hot water load over one year in case study building.

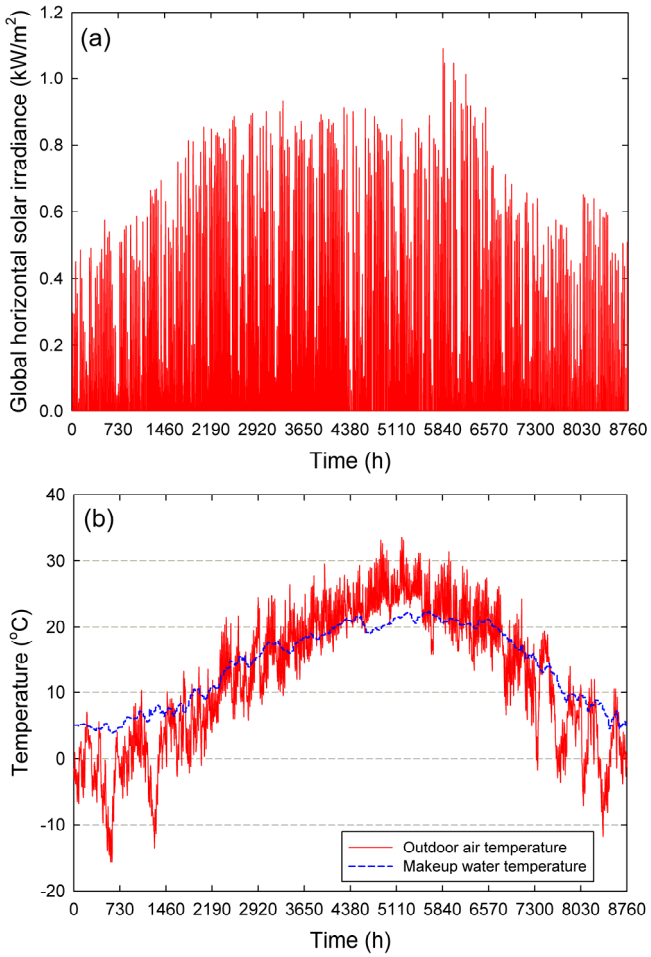

Figure 4. (**a**) Hourly global horizontal solar irradiance and (**b**) outdoor air temperature and makeup water temperature over one year in Incheon, South Korea.

Table 1. Optimization parameters considered in case study.

Parameter	Description	Value
γ	Azimuth of collector array (°)	0
$\alpha_{s,w}$	Meridian altitude in winter (°)	29
T_l	Desired hot water temperature (°C)	60
$T_{s,max}$	Maximum allowable storage tank temperature (°C)	100
T_{amb}	Temperature of environment surrounding storage tank (°C)	20
$N_{coll,s,max}$	Maximum number of collectors in series (ea.)	6
$C_{p,c}$	Specific heat of collector fluid (J/kg· °C)	3843
$C_{p,w}$	Specific heat of water (J/kg· °C)	4153
ρ_{coll}	Density of collector fluid (kg/m^3)	1032
ρ_w	Density of water (kg/m^3)	991
ρ_g	Ground reflectance (-)	0.2
ΔT_{on}	Upper deadband temperature difference of DTC (°C)	8
ΔT_{off}	Lower deadband temperature difference of DTC (°C)	2
η_p	Pumping efficiency of circulation pump (%)	60
η_m	Motor efficiency of circulation pump (%)	80
$H_{p,h}$	Head of pump on hot side of heat exchanger (m)	80
$H_{p,c}$	Head of pump on cold side of heat exchanger (m)	15
$H_{p,l}$	Head of pump on load side of SWH system (m)	80
n_p	Planning period (years)	40
i	Real discount rate (%)	2.91
e_{ELE}	Electricity cost escalation rate (%)	4.00
e_{LNG}	Gas cost escalation rate (%)	4.00
$A_{R,max}$	Maximum capacity available to receive subsidy cost (m^2)	500
$A_{coll,max}$	Area available to install solar collectors (m^2)	600
R_I	Supplementary cost ratio against purchase cost (%)	30
R_M	Maintenance cost ratio against initial cost (%)	1.5
R_S	Subsidy cost ratio against initial cost (%) [42]	50

Table 2. Electricity and liquid natural gas(LNG) tariffs.

Classification			Value
Electricity	Energycharge (KRW/kW·h)	Basic charge	6160
		Summer (June, July, and August)	105.7
		Spring/fall (March, April, May, September, and October)	65.2
		Winter (November, December, January, and February)	92.3
LNG	Energycharge (KRW/MJ)	Summer (May, June, July, August, and September)	19.26
		Spring/fall (April, October, and November)	19.28
		Winter (December, January, February, and March)	19.46

4.2. Multi-Objective Optimization Results

Figure 5 shows the evolution of the Pareto frontiers, which are the corresponding objective function values of the non-dominated solutions, for different numbers of generation. As shown in Figure 5, the Pareto frontiers are mainly improved at the beginning of the optimization process (until approximately the 500th generation). In the subsequent generations, the improvements in the objective function values are insignificant. Therefore, 3000 generations can be considered as a fair termination condition for the optimization process. The values of the LCC and LCES for the last generation are 216.7–280.6 million KRW (approximately 182.4–236.1 thousand USD) and 1461.4–1923.1 MWh, respectively. Compared to the average values of the LCC and LCES of the solutions in the initial population, the solution with the lowest LCC (the lowest LCES) reduces the cost by 24.1% and even the solution with the highest LCC (the highest LCES) reduces the cost by 1.7%. Furthermore, the solutions with the lowest LCES and highest LCES increase the energy saving by 7.7% and 41.8%, respectively.

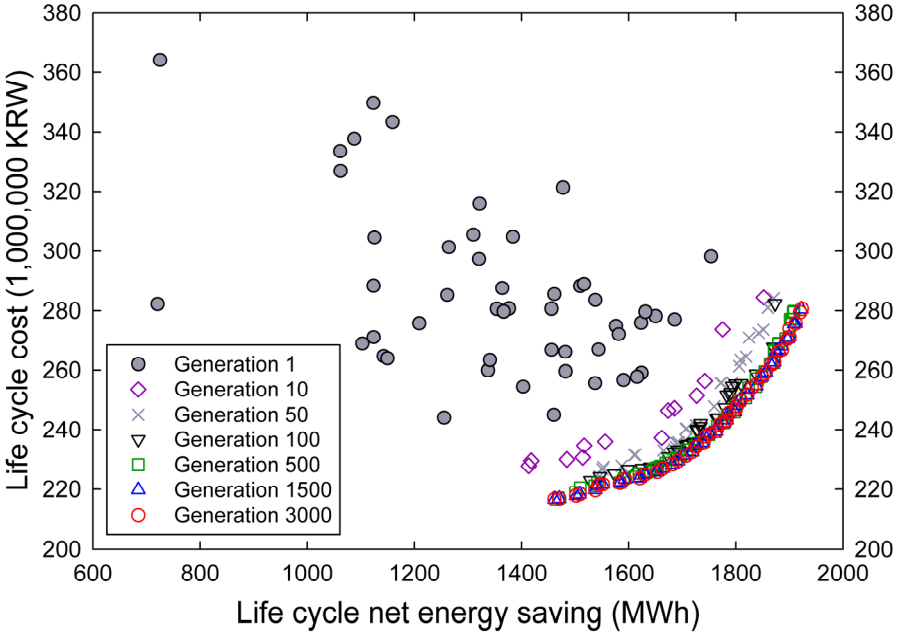

Figure 5. Evolution of Pareto frontier through many generations.

Figure 6, which shows the Pareto frontier in the last generation, reveals the conflict between two objectives: the LCC and LCES. The multi-objective optimization involving the simultaneous maximization of the LCES and minimization of the LCC corresponds to the Max-Min problem, whose convex shape appears to curve toward the bottom right direction. Therefore, the optimization results from the case study show an appropriate trade-off.

To investigate the characteristics of the non-dominated solutions, the correlation between the LCC and LCES is analyzed by the regression technique. According to the linear regression analysis, as shown in Figure 6, the Pareto frontier can be divided into four clusters—Clusters 1–4—which are groups with similar characteristics. Each coefficient (slope of the linear fit) appears as a percentage of the increase in the LCC for an increase in the LCES, and this means that the larger the coefficient, the greater is the cost required to increase the energy saving by the SWH system. The R^2 indexes for the output from the linear regression of Clusters 1–4 show good linearity. The coefficients obtained for Clusters 1–4 are 0.049, 0.110, 0.195, and 0.302 million KRW/MWh, respectively. In other words, the non-dominated solutions in Cluster 1 require an additional LCC of 490 thousand KRW to save 1 MWh of energy over 40 years. The additional costs of non-dominated solutions in Clusters 2–4 increase by 124.5%, 298.0%, and 516.3%, respectively, compared to that in Cluster 1.

The LCC can be divided into the energy cost and equipment cost, which represents the cost obtained by subtracting the subsidy cost from the sum of the initial, maintenance, and replacement costs. A trade-off between the energy and equipment costs results in an optimal economic design of the SWH system. Figure 7 shows the correlations between these costs and the LCES, and the output from the linear regression of Clusters 1–4. As shown in Figure 7, the linear regression lines between the LCES and energy cost for Clusters 1–4 have similar coefficients, ranging between −0.120 and −0.134 million KRW/MWh, even though the coefficient for Cluster 3 is slightly lower than those for Clusters 1, 2, and 4. However, the coefficients of the linear fit between the LCES and equipment cost for Clusters 1–4 are 0.169, 0.231, 0.329, and 0.422 million KRW/MWh, respectively; that is, they are very different. From this regression analysis, it is found that the energy cost of the non-dominated solutions decreases linearly in similar proportions with an increase in the LCES, regardless of the classification of the cluster. However, the equipment cost of the non-dominated solutions increases more significantly as the LCES increases. Therefore, a trade-off between the LCES and LCC of the non-dominated solutions is mainly caused by the variation in the equipment cost.

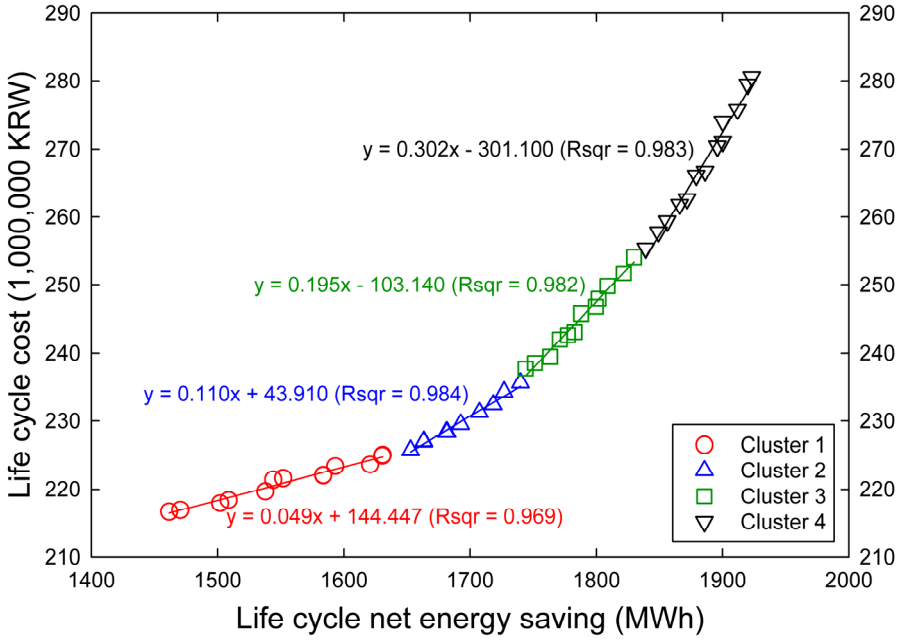

Figure 6. Pareto frontier for last generation in case study.

The decision variables and some key information corresponding to each cluster are presented in Table 3. All clusters have the common trend that the solar fractions increase and the system efficiencies decrease as the LCES increases. This is because at high solar fractions in the SWH systems, increasingly larger component capacities are required to further increase the solar fraction. In other words, by employing additional solar collectors or a larger storage tank and heat exchanger, more energy than that required to increase the solar fraction is supplied to the storage tank, and the remaining heat is used to keep the storage tank temperature high for a long time. However, because the high temperature of the storage tank increases the heat loss to the ambient air and discharges heat to avoid overheating, the efficiency of the SWH system decreases. The solar fractions of the non-dominated solutions at the last generation are considerably high, ranging from 66.7% to 87.1%. As can be seen from Table 3, the capacities of the main components except for the auxiliary heater, which is selected to have the same capacity of 34.89 kW because of its high efficiency, increase as the LCES increases, but the increasing trend is not constant. It is also found that the collector slope increases with an increase in the LCES because it is more efficient to increase the solar fraction during the winter than in the summer or the intermediate season, when the solar fraction is very close to the upper limit. Overall, the mass flow rate per unit area of the collector fluid ($m_{coll,u}$) decreases with an increase in the LCES, but the minimum and maximum $m_{coll,u}$ values are 28.8 and 50.4 kg/s·m^2, respectively; these values are in agreement with the results of previous studies, e.g., 50 kg/h·m^2 [43], 18–48 kg/h·m^2 [44], and 20–40 kg/h·m^2 [21]. As the mass flow rate-to-collector area ratio, the mass flow rates on the cold side of the heat exchanger ($m_{hex,c}$) for Clusters 1–4 are 0.0039–0.0049, 0.0033–0.0039, 0.0031–0.0035, and 0.0025–0.0038 kg/s·m^2, respectively. These values are in agreement with the typically known range of values: 0.002–0.008 kg/s·m^2 [13]. Similar to the variation in $m_{coll,u}$, $m_{hex,c}$ decreases with an increase in the LCES, but a clear decreasing trend is not found.

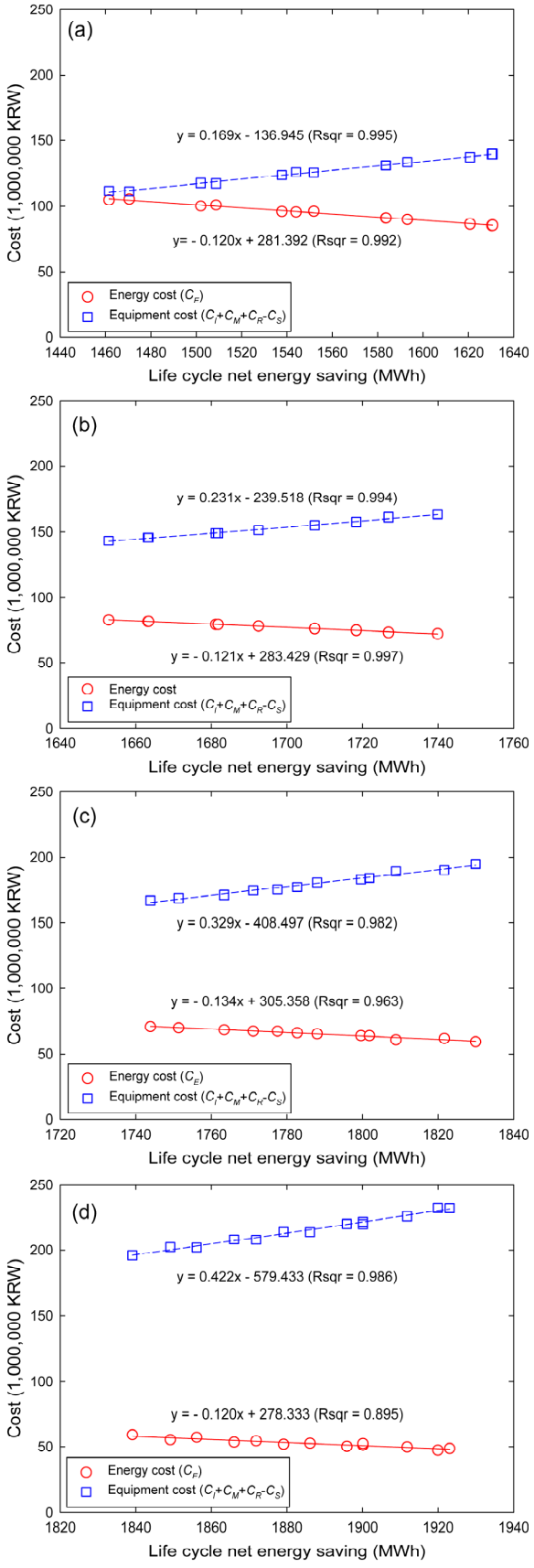

Figure 7. Correlation between cost and energy saving of Pareto frontier for last generation: (**a**) Cluster 1; (**b**) Cluster 2; (**c**) Cluster 3; and (**d**) Cluster 4.

Table 3. Characteristics of non-dominated solutions for last generation for different clusters.

Parameter	Classification			
	Cluster 1	**Cluster 2**	**Cluster 3**	**Cluster 4**
T_{coll} (-)	4	4	4	4
N_{coll} (ea.)	73–85	91–109	115–139	127–163
$A_{coll,j} \cdot N_{coll}$ (m^2)	144.54–168.30	180.18–215.82	227.70–275.22	251.46–322.74
T_{hex} (-)	1–2	2	2–5	3–5
UA_{hex} (W/°C)	3489–4071	4071	4071–5815	4652–5815
T_{tank} (-)	2–6	5–6	5–7	7
V_s (m^3)	3.76–6.92	6.21–6.92	6.21–9.58	9.58
T_{aux} (-)	4	4	4	4
N_{aux} (ea.)	1	1	1	1
$q_{aux,j} \cdot N_{aux}$ (kW)	34.89	34.89	34.89	34.89
β_{coll} (°)	35–37	37–39	38–42	41–43
$m_{coll,u}$ (kg/s· m^2)	0.011–0.014	0.010–0.011	0.009–0.010	0.008–0.011
$m_{hex,c}$ (kg/s)	0.604–0.707	0.686–0.746	0.712–0.910	0.791–1.029
F_S (%)	66.7–73.9	74.8–78.2	78.8–83.0	82.8–87.1
η_{sys} (%)	17.4–19.5	15.4–17.7	12.9–15.2	11.5–14.1
C_E (million KRW)	85.4–105.5	72.3–82.7	59.1–70.8	47.4–59.3
$C_I + C_M + C_R - C_S$ (million KRW)	111.5–139.5	143.1–163.4	166.9–195.0	196.0–232.1
C_{LCC} (million KRW)	216.7–225.1	225.8–235.6	237.7–254.1	255.4–280.6
Q_{LCES} (MWh)	1461.5–1630.7	1652.8–1739.9	1743.9–1829.9	1839.1–1923.1

4.3. Characteristics of Non-Dominated Solutions according to RVA

Although each solution belonging to the group of Pareto optimal solutions is potentially a best solution, to enable designers and engineers to select one particular solution based on their specific requirement, the corresponding energy performance parameters such as the solar fraction and system efficiency should be evaluated. Figure 8 shows the variations in the solar fraction and system efficiency of the non-dominated solutions at the last generation with an increase in the LCES. As expected, it is found that the solar fraction of the non-dominated solutions increases linearly with an increase in the LCES, regardless of the classification of the cluster. However, although the overall system efficiency tends to decrease, the decreasing trends of the non-dominated solutions in the same cluster are different. In other words, each cluster includes some system configurations that show different characteristics in terms of the energy and economic performance.

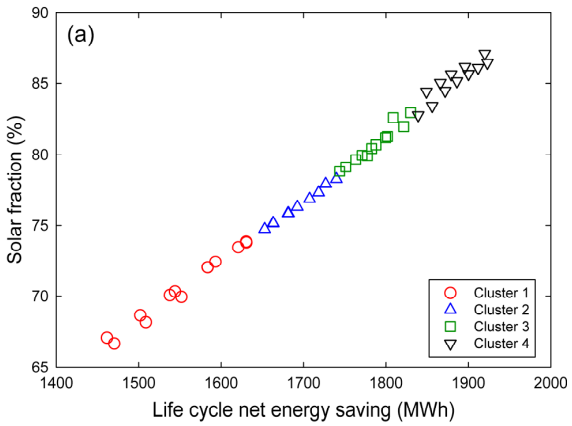

Figure 8. *Cont.*

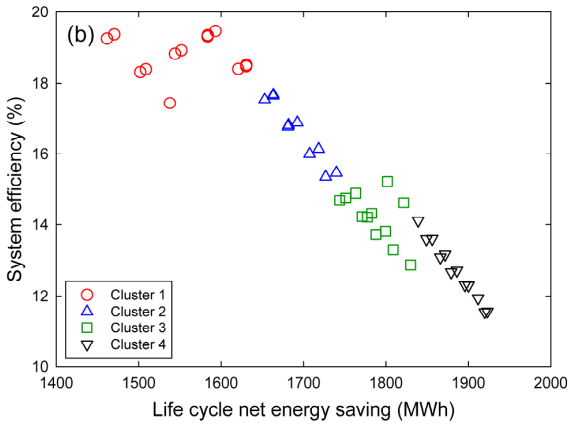

Figure 8. Correlation between LCES and energy performance of non-dominated solutions for last generation: (**a**) solar fraction *vs.* LCES and (**b**) system efficiency *vs.* LCES.

To analyze the variation in the characteristics of the SWH systems obtained by the proposed optimization method in more detail, the configurations of non-dominated solutions and their corresponding energy and economic performance are evaluated using the RVA. The solar collectors and storage tanks are recognized as the most important components in terms of the energy and economic performance of the SWH system. Furthermore, this performance of the SWH system can often be parameterized using the relationship between these two components [45]. First, all non-dominated solutions are divided into five groups according to the five types of storage tanks included in their configurations. Then, the variations in the energy and economic performance depending on the RVA are analyzed. As shown in Figure 9, the non-dominated solutions belonging to each group, which consist of the solutions with the same storage tank, show a common pattern of variation in the energy and economic performance depending on the RVA. It can be seen that in all the groups, the solar fraction increases linearly with a decrease in the RVA—that is, an increase in the collector area, because of the accompanied increase in the storage tank temperature. However, the system efficiency decreases linearly with a decrease in the RVA because of the energy loss caused by keeping the storage tank temperature high. Furthermore, the two objective functions vary with the RVA while maintaining good correlations. For the same reason as that mentioned for the variation in the solar fraction, the LCES increases linearly with a decrease in the RVA. The LCC decreases with an increase in the RVA, which leads to an increase in the system efficiency, but their correlations are expressed by the quadratic regression model because of the variation in the equipment cost. It is also found that the rates of variation for the solar fraction, system efficiency, and LCES increase as the storage tank volume decreases, whereas that for the LCC does not. In addition, the values of the RVA for all non-dominated solutions range from 22 to 45 L/m^2; these values are in agreement with the results of a previous study [8].

Figure 10 presents the distribution of the Pareto frontier of the last generation according to the five groups that are divided by the storage tank volume in Figure 9. The Pareto frontiers belonging to each group are widely spread unlike the distribution of each cluster divided by the trade-off between the objective function values. From Figures 6 and 10 it is also found that each cluster includes some system configurations that are characterized by the variation in the RVA depending on the storage tank volume. Therefore, when selecting the best solution from among the non-dominated solutions, it is necessary to consider the trade-off between the objective function values in conjunction with the energy performance of the SWH system depending on the RVA. For example, as shown in Figure 10 and Table 4, Solutions 1–3, which are composed of substantially same decision variables except for the collector area and storage tank volume, have very similar objective function values. However, a decision maker can make the SWH system more efficient by selecting Solution 3, whose RVA is greater than those of the other two solutions, while increasing the LCC only by less than 1%.

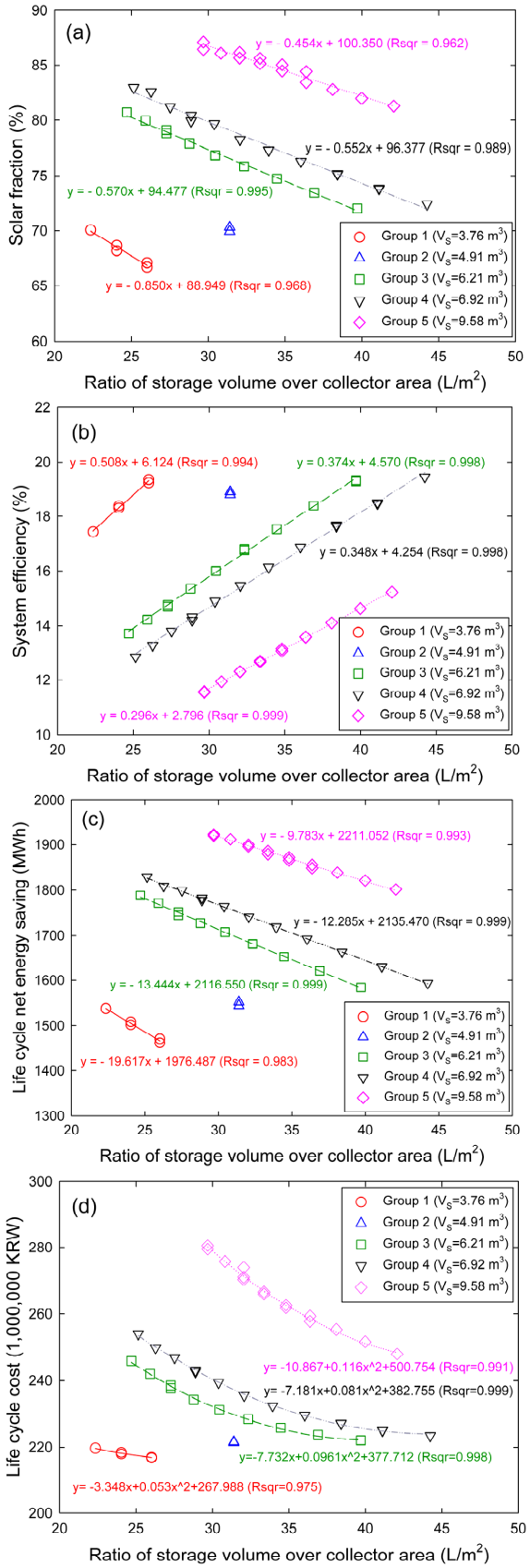

Figure 9. Correlations between energy and economic performance and RVA: (**a**) solar fraction *vs.* RVA; (**b**) system efficiency *vs.* RVA; (**c**) LCES *vs.* RVA; and (**d**) LCC *vs.* RVA.

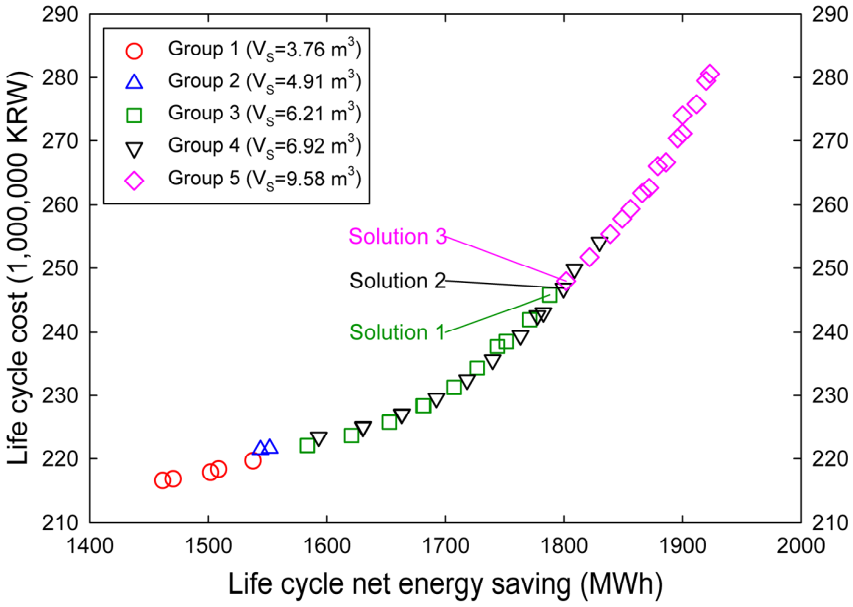

Figure 10. Pareto frontier for last generation divided by storage tank volume.

Table 4. Characteristics of three non-dominated solutions considered in Figure 10.

Parameter	Classification		
	Solution 1	Solution 2	Solution 3
T_{coll} (-)	4	4	4
N_{coll} (ea.)	127	127	115
$A_{coll,j} \cdot N_{coll}$ (m^2)	251.46	251.46	227.70
T_{hex} (-)	3	3	3
UA_{hex} (W/°C)	4652	4652	4652
T_{tank} (-)	5	6	7
V_s (m^3)	6.21	6.92	9.58
T_{aux} (-)	4	4	4
N_{aux} (ea.)	1	1	1
$q_{aux,j} \cdot N_{aux}$ (kW)	34.89	34.89	34.89
β_{coll} (°)	41	41	40
$m_{coll,u}$ (kg/s·m^2)	0.009	0.009	0.010
$m_{hex,c}$ (kg/s)	0.791	0.791	0.775
RVA (liter/m^2)	24.70	27.52	42.07
F_S (%)	80.7	81.2	81.3
η_{sys} (%)	13.7	13.8	15.2
C_E (million KRW)	65.23	63.84	63.81
$C_I + C_M + C_R - C_S$ (million KRW)	180.58	182.98	184.13
C_{LCC} (million KRW)	245.81	246.82	247.94
Q_{LCES} (MWh)	1787.98	1799.58	1801.82

5. Conclusions

This study investigated the multi-objective optimization method for an indirect forced-circulation SWH system to determine the optimal configuration that would maximize the benefits from the energy and economic perspectives. NSGA-II was employed to determine the optimal configuration by minimizing the LCC and maximizing the LCES of the SWH system. The proposed optimization method was applied to the design of the SWH system of an office building in Incheon, South Korea. The optimization results from the case study show that there is an appropriate trade-off between the LCC and LCES. By performing the regression technique on the Pareto frontier obtained from the optimization, it is found that the energy cost decreases linearly and the equipment

cost increases more significantly as the LCES increases. However, the results also show that it is difficult to identify a trend in the energy and economic performance for the Pareto optimal solutions using only the correlation between the corresponding objective function values. Therefore, the effect of the RVA on the energy and economic performance of the non-dominated solutions was analyzed. The results indicate that the performance of the non-dominated solutions, which have the same storage tank volume, varies with the RVA, while maintaining good correlations. Therefore, it is necessary to simultaneously consider the trade-off between the objective function values and the effect of the RVA while selecting the best solution from among the Pareto optimal solutions.

Acknowledgments: This work was supported by the National Research Foundation of Korea (NRF) grant funded by the Korea government (MSIP) (NRF-2014R1A6A3A01059739).

Conflicts of Interest: The author declares no conflict of interest.

Nomenclature

A_{coll}	gross area of a single collector module, m^2
$A_{coll,j}$	gross area of the jth device of solar collectors, m^2
$A_{coll,max}$	area available to install solar collectors, m^2
$A_{R,max}$	maximum capacity available to receive the subsidy cost, m^2
A_s	surface area of a storage tank, m^2
$C_{hex,c}$	capacity rate of fluid on cold side of a heat exchanger, $W/^\circ C$
$C_{hex,h}$	capacity rate of fluid on hot side of a heat exchanger, $W/^\circ C$
$C_{hex,max}$	maximum capacity rate, $W/^\circ C$
$C_{hex,min}$	minimum capacity rate, $W/^\circ C$
$C_{p,w}$	specific heat of water, $J/kg\cdot ^\circ C$
$C_{p,c}$	specific heat of collector fluid, $J/kg\cdot ^\circ C$
$C_{aux,j}$	purchase cost of the jth auxiliary heater, KRW
$C_{coll,j}$	purchase cost of the jth solar collector, KRW
$C_{hex,j}$	purchase cost of the jth heat exchanger, KRW
$C_{tank,j}$	purchase cost of the jth storage tank, KRW
C_E	energy cost, KRW
C_I	initial cost, KRW
$C_{I,c}$	initial cost of each component, KRW
C_M	maintenance cost, KRW
C_R	replacement cost, KRW
$C_{R,c}$	replacement cost of each component, KRW
C_S	subsidy cost, KRW
C_{LCC}	life cycle cost, KRW
c_{ELE}	hourly electricity cost, KRW/kWh
c_{LNG}	hourly liquid natural gas (LNG) cost, KRW/m^3
c_r	capacity rate ratio of a heat exchanger
e_{fuel}	fuel price escalation rate, %
$EIR\,(PLR_{aux})$	energy input ratio of the auxiliary heaters
F_{ELE}	hourly electricity consumption of the circulation pump, kWh
F_{LNG}	hourly LNG consumption of the auxiliary heaters, m^3
$F_R\,(\tau\alpha)$	intercept of the efficiency curve of identical collector modules connected in series
$F_{R1}\,(\tau\alpha)_1$	intercept of the efficiency curve of a single collector
$F_R U_L$	slope of the efficiency curve of identical collector modules connected in series, $W/m^2\cdot ^\circ C$

$F_{R1}U_{L1}$	slope of the efficiency curve of a single collector, W/m$^2\cdot$ °C
F_S	solar fraction of the solar system over a given time horizon, %
g	acceleration due to gravity, m/s^2
$H_{coll,j}$	height of the jth device of solar collectors, m
H_p	circulation pump head, m
I	global solar radiation on a horizontal surface, W/m^2
I_b	hourly beam solar radiation on a horizontal surface, W/m^2
I_d	hourly diffuse solar radiation on a horizontal surface, W/m^2
I_T	hourly total solar radiation on the tilted collector array, W/m^2
i	real discount rate, %
$m_{coll,u}$	mass flow rate per unit area of the collector fluid, kg/s$\cdot$ m^2
$m_{hex,c}$	mass flow rate on the cold side of the heat exchanger, kg/s
m_d	mass flow rate of the discharged water from a storage tank, kg/s
m_{fluid}	mass flow rate of the fluid passing through the pump, kg/s
m_s	mass flow rate from the storage tank to the load, kg/s
m_l	mass flow rate of the desired hot water load, kg/s
$N_{coll,p}$	number of parallel connections in the collector array
$N_{coll,s}$	number of identical collectors in series
$N_{coll,s,max}$	maximum number of identical collectors in series
N_{coll}	number of the jth devices of solar collectors
N_{aux}	number of the jth devices of auxiliary heaters
NTU	number of exchanger heat transfer units
n_p	planning period, year
$n_{l,c}$	life span of each component, year
$n_{r,c}$	Number of times each component is replaced
PEF_{ELE}	primary energy factor for electricity
PLR_{aux}	part load ratio of the auxiliary heaters at each time step
$q_{aux,j}$	heating capacity of the jth device of auxiliary heaters, kW
$Q_{aux,total}$	total heating capacity of the auxiliary heaters, kW
Q_L	hourly hot water load, Wh
Q_{LCES}	life cycle net energy cost of the solar system over the planning period, MWh
$q_{L,peak}$	peak hot water load, kW
$Q_{LNG,LHV}$	lower heating value of LNG, m^3/W
q_{aux}	auxiliary heating energy, W
q_d	discharged heat to avoid overheating of a storage tank, W
q_l	heat loss of a storage tank, W
q_{Ls}	solar energy extracted from the storage tank to the load, W
q_{hex}	solar energy supplied to a storage tank, W
q_u	solar useful heat gain of identical collectors in series, W
R_b	the ratio of the beam radiation on the tilted surface to that on a horizontal surface
R_I	percentage of the supplementary cost against the direct purchase cost, %
R_M	percentage of the annual maintenance cost against the initial cost, %
R_S	percentage of subsidy cost against the initial cost, %
T_a	outdoor dry-bulb temperature, °C
T_{amb}	ambient temperature, °C
T_{ci}	cold stream inlet temperature of a heat exchanger, °C
T_{co}	cold stream outlet temperature of a heat exchanger, °C
T_H	upper input temperature of the differential temperature controller (DTC), °C
T_{hi}	hot stream inlet temperature of a heat exchanger, °C
T_{ho}	hot stream outlet temperature of a heat exchanger, °C

T_L	lower input temperature of the DTC, °C
T_l	desired hot water temperature, °C
T_m	make-up water temperature, °C
T_s	storage tank temperature at the beginning of the time step, °C
$T_{s,f}$	storage tank temperature at the end of the time step, °C
$T_{s,max}$	maximum allowable storage tank temperature, °C
T_{aux}	type of auxiliary heater
T_{coll}	type of solar collector
T_{hex}	type of heat exchanger
T_{tank}	type of storage tank
U_s	heat loss coefficient of a storage tank, W/m$^2\cdot$°C
UA_{hex}	product of the overall heat transfer coefficient and area of a heat exchanger, W/°C
UPA^*_{ELE}	uniform present value factor adjusted to reflect the electricity price escalation rate
UPA^*_{LNG}	uniform present value factor adjusted to reflect the LNG price escalation rate
UPA^*_{fuel}	uniform present value factor adjusted to reflect the fuel price escalation rate
V_s	storage tank volume, m^3
$W_{coll,j}$	width of the *j*th device of solar collectors, m
$\alpha_{s,w}$	meridian altitude in winter, °
β_{coll}	slope of the collector array, °
γ_o	output control function of the DTC
ε	effectiveness of a heat exchanger
η_{aux}	overall efficiency of auxiliary heater
η_m	motor efficiency of circulation pump
η_p	pumping efficiency of circulation pump
η_{sys}	efficiency of the solar system over a given time horizon
ρ_g	ground reflectance
ρ_w	density of water, kg/m^3
ΔT_{on}	upper deadband temperature difference of the DTC, °C
ΔT_{off}	lower deadband temperature difference of the DTC, °C

Appendix

Table A1. Technical and economic parameters of solar collectors for case study.

Parameters	Types				
	0	**1**	**2**	**3**	**4**
Interceptofcollectorefficiency (-)	0.7445	0.7208	0.7200	0.7109	0.7043
Negative ofslopeofcollectorefficiency (W/m$^2\cdot$°C)	4.8483	4.7999	4.0900	5.0050	4.5368
Flow rate of fluid understandardconditions (kg/s)	0.0381	0.0373	0.0400	0.0368	0.0368
Overall height (m)	2.00	2.00	2.00	2.02	2.00
Overall width (m)	1.00	1.00	1.00	1.00	0.99
Life span (year)	20	20	20	20	20
Purchasecost (1000 KRW/ea.)	545	530	520	545	540

Table A2. Technical and economic parameters of heat exchangers for case study.

Parameters	Types							
	0	**1**	**2**	**3**	**4**	**5**	**6**	**7**
Overall heat transfer coefficient-area product (W/°C)	2908	3489	4071	4652	5234	5815	6978	8141
Total heat transfer area (m^2)	0.8398	1.0608	1.2376	1.4000	1.5400	1.6800	2.1000	2.3800
Area per plate (m^2)	0.0442	0.0442	0.0442	0.1400	0.1400	0.1400	0.1400	0.1400
Total number of plates	21	26	30	12	13	14	17	19
Life span (year)	5	5	5	5	5	5	5	5
Purchase cost (1000 KRW/ea.)	670	730	780	1050	1070	1100	1170	1220

Table A3. Technical and economic parameters of storage tanks for case study.

Parameters	Types							
	0	**1**	**2**	**3**	**4**	**5**	**6**	**7**
Tank volume (m^3)	1.72	2.65	3.76	4.91	5.54	6.21	6.92	9.58
Heatlosscoefficient (W/°C)	0.3	0.3	0.3	0.3	0.3	0.3	0.3	0.3
Overall height (m)	1.52	2.00	2.44	2.44	2.44	2.44	3.05	3.05
Overall diameter (m)	1.20	1.30	1.40	1.60	1.70	1.80	1.70	2.00
Life span (year)	15	15	15	15	15	15	15	15
Purchasecost (1,000,000 KRW/ea.)	9.49	10.73	12.65	15.88	17.33	18.02	18.98	24.00

Table A4. Technical and economic parameters of auxiliary heaters for case study.

Parameters	Types					
	0	**1**	**2**	**3**	**4**	**5**
Rated heating capacity (kW)	15.12	18.61	23.26	29.08	34.89	58.15
Rated efficiency (%)	83	84	85	86	86	82
Life span (year)	15	15	15	15	15	15
Purchase cost (1000 KRW/ea.)	807	844	909	964	1039	2291

References

1. Hottel, H.C.; Whillier, A. *Evaluation of Flat-Plate Collector Performance*; University of Arizona Press: Tucson, AZ, USA, 1958.
2. Klein, S.A. Calculation of flat-plate collector utilizability. *Sol. Energy* **1978**, *21*, 393–402.
3. Klein, S.A.; Beckman, W.A.; Duffie, J.A. A design procedure for solar heating systems. *Sol. Energy* **1976**, *18*, 113–127. [CrossRef]
4. Klein, S.A.; Beckman, W.A. A general design method for closed-loop solar energy systems. *Sol. Energy* **1979**, *22*, 269–282. [CrossRef]
5. Klein, S.A.; Cooper, P.I.; Freeman, T.L.; Beekman, D.L.; Beckman, W.A.; Duffie, J.A. A method of simulation of solar processes and its application. *Sol. Energy* **1975**, *17*, 29–37. [CrossRef]
6. Lund, P.D.; Peltola, S.S. SOLCHIPS—A fast predesign and optimization tool for solar heating with seasonal storage. *Sol. Energy* **1992**, *48*, 291–300. [CrossRef]
7. Atia, D.M.; Fahmy, F.H.; Ahmed, N.M.; Dorrah, H.T. Optimal sizing of a solar water heating system based on a genetic algorithm for an aquaculture system. *Math. Comput. Model* **2012**, *55*, 1436–1449. [CrossRef]
8. Matrawy, K.K.; Farkas, I. New technique for short term storage sizing. *Renew. Energy* **1997**, *11*, 129–141. [CrossRef]
9. Michelson, E. Multivariate optimization of a solar water heating system using the Simplex method. *Sol. Energy* **1982**, *29*, 89–99. [CrossRef]
10. Loomans, M.; Visser, H. Application of the genetic algorithm for optimization of large solar hot water systems. *Sol. Energy* **2002**, *72*, 427–439. [CrossRef]

11. Krause, M.; Vajen, K.; Wiese, F.; Ackermann, H. Investigation on optimizing large solar thermal systems. *Sol. Energy* **2002**, *73*, 217–225. [CrossRef]
12. Kalogirou, S.A. Optimization of solar systems using artificial neural-networks and genetic algorithms. *Appl. Energy* **2004**, *77*, 383–405. [CrossRef]
13. Kim, Y.D.; Thu, K.; Bhatia, H.K.; Bhatia, C.S.; Ng, K.C. Thermal analysis and performance optimization of a solar hot water plant with economic evaluation. *Sol. Energy* **2012**, *86*, 1378–1395. [CrossRef]
14. Ko, M.J. Analysis and optimization design of a solar water heating system based on life cycle cost using a genetic algorithm. *Energies* **2015**, *8*, 11380–11403. [CrossRef]
15. Ko, M.J. A novel design method for optimizing an indirect forced circulation solar water heating system based on life cycle cost using a genetic algorithm. *Energies* **2015**, *8*, 11592–11617. [CrossRef]
16. Bornatico, R.; Pfeiffer, M.; Witzig, A.; Guzzella, L. Optimal sizing of a solar thermal building installation using particle swarm optimization. *Energy* **2012**, *41*, 31–37. [CrossRef]
17. Sadafi, M.H.; Hosseini, R.; Safikhani, H.; Bagheri, A.; Mahmoodabadi, M.J. Multi-objective optimization of solar thermal energy storage using hybrid of particle swarm optimization, multiple crossover and mutation operator. *Int. J. Eng. Trans. B* **2011**, *24*, 367–376. [CrossRef]
18. Cheng Hin, J.N.; Zmeureanu, R. Optimization of a residential solar combisystem for minimum life cycle cost, energy use and exergy destroyed. *Sol. Energy* **2014**, *100*, 102–113. [CrossRef]
19. Kusyy, O.; Kuethe, S.; Vajen, K. Simulation-based optimization of a solar water heating system by a hybrid genetic-binary search algorithm. In Proceedings of the 2010 Xvth International Seminar/Workshop on Direct and Inverse Problems of Electromagnetic and Acoustic Wave Theory (DIPED), Tbilisi, GA, USA, 27–30 September 2010; IEEE: Piscataway, NJ, USA.
20. Shariah, A.M.; Löf, G.O.G. The optimization of tank-volume-to-collector-area ratio for a thermosyphon solar water heater. *Renew. Energy* **1996**, *7*, 289–300. [CrossRef]
21. Hobbi, A.; Siddiqui, K. Optimal design of a forced circulation solar water heating system for a residential unit in cold climate using TRNSYS. *Sol. Energy* **2009**, *83*, 700–714. [CrossRef]
22. Yan, C.; Wang, S.; Ma, Z.; Shi, W. A simplified method for optimal design of solar water heating systems based on life-cycle energy analysis. *Renew. Energy* **2015**, *74*, 271–278. [CrossRef]
23. Lima, J.B.A.; Prado, R.T.A.; Taborianski, V.M. Optimization of tank and flat-plate collector of solar water heating system for single-family households to assure economic efficiency through the TRNSYS program. *Renew. Energy* **2006**, *31*, 1581–1595. [CrossRef]
24. Choi, D.S.; Ko, M.J. Optimization design for a solar water heating system using the genetic algorithm. *Int. J. Appl. Eng. Res.* **2015**, *10*, 27031–27042.
25. Kulkarni, G.N.; Kedare, S.B.; Bandyopadhyay, S. Determination of design space and optimization of solar water heating systems. *Sol. Energy* **2007**, *81*, 958–968. [CrossRef]
26. Kulkarni, G.N.; Kedare, S.B.; Bandyopadhyay, S. Optimization of solar water heating systems through water replenishment. *Energy Convers. Manag.* **2009**, *50*, 837–846. [CrossRef]
27. Deb, K. *Multi-Objective Optimization Using Evolutionary Algorithms*; Wiley: Chichester, UK, 2009.
28. Konak, A.; Coit, D.W.; Smith, A.E. Multi-objective optimization using genetic algorithms: A tutorial. *Reliab. Eng. Syst. Saf.* **2006**, *91*, 992–1007. [CrossRef]
29. Li, Y.; Liao, S.; Liu, G. Thermo-economic multi-objective optimization for a solar-dish Brayton system using NSGA-II and decision making. *Int. J. Electr. Power Energy Syst.* **2015**, *64*, 167–175. [CrossRef]
30. Ahmadi, M.H.; Dehghani, S.; Mohammadi, A.H.; Feidt, M.; Barranco-Jimenez, M.A. Optimal design of a solar driven heat engine based on thermal and thermo-economic criteria. *Energy Convers. Manag.* **2013**, *75*, 635–642. [CrossRef]
31. Khorasaninejad, E.; Hajabdollahi, H. Thermo-economic and environmental optimization of solar assisted heat pump by using multi-objective particle swarm algorithm. *Energy* **2014**, *72*, 680–690. [CrossRef]
32. Gebreslassie, B.H.; Jimenez, M.; Guillén-Gosálbez, G.; Jiménez, L.; Boer, D. Multi-objective optimization of solar assisted absorption cooling system. *Comput. Aided Chem. Eng.* **2010**, *28*, 1033–1038.
33. Gebreslassie, B.H.; Guillén-Gosálbez, G.; Jiménez, L.; Boer, D. Solar assisted absorption cooling cycles for reduction of global warming: A multi-objective optimization approach. *Sol. Energy* **2012**, *86*, 2083–2094. [CrossRef]
34. Wang, M.; Wang, J.; Zhao, P.; Dai, Y. Multi-objective optimization of a combined cooling, heating and power system driven by solar energy. *Energy Convers. Manag.* **2015**, *89*, 289–297. [CrossRef]

35. Hang, Y.; Du, L.; Qu, M.; Peeta, S. Multi-objective optimization of integrated solar absorption cooling and heating systems for medium-sized office buildings. *Renew. Energy* **2013**, *52*, 67–78. [CrossRef]
36. Boyaghchi, F.A.; Heidarnejad, P. Thermoeconomic assessment and multi objective optimization of a solar micro CCHP based on Organic Rankine Cycle for domestic application. *Energy Convers. Manag.* **2015**, *97*, 224–234. [CrossRef]
37. Duffie, J.A.; Beckman, W.A. *Solar Engineering of Thermal Processes*, 3rd ed.; Wiley: Hoboken, NJ, USA, 2006.
38. Henderson, H.; Huang, Y.J.; Parker, D. *Residential Equipment Part Load Curve for Use in DOE-2: Technical Report LBNL-42175*; Lawrence Berkeley National Laboratory: Berkeley, CA, USA, 1999.
39. Deb, K.; Pratap, A.; Agarwal, S.; Meyarivan, T. A fast and elitist multiobjective genetic algorithm: NSGA-II. *IEEE Trans. Evol. Comput.* **2002**, *6*, 182–197. [CrossRef]
40. Kanpur Genetic Algorithms Laboratory. Available online: http://www.iitk.ac.in/kangal/codes.shtml (accessed on 29 January 2015).
41. National Renewable Energy Laboratory. Available online: http://www.nrel.gov/docs/fy11osti/46861.pdf (accessed on 29 January 2015).
42. Korea Law. Available online: http://www.law.go.kr (accessed on 16 October 2015).
43. Beckman, W.A.; Klein, S.A.; Duffie, J.A. *Solar Heating Design by the F-Chart Method*; John Wiley: New York, NY, USA, 1977.
44. Baughn, J.W.; Young, M.F. The calculated performance of a solar hot water system for a range of collector flow rates. *Sol. Energy* **1984**, *32*, 303–305. [CrossRef]
45. Lund, P.D.; Keinonen, R.S. *Economic analysis of central solar heating systems with seasonal storage: Report TKK-F-A589*; Helsinki University of Technology: Espoo, Finland, 1985.